

Active Young-Dupré Equation: How Self-organized Currents Stabilize Partial Wetting

Yongfeng Zhao^{1,2,†}, Ruben Zakine³, Adrian Daerr³, Yariv Kafri⁴, Julien Tailleur^{5,3}, Frédéric van
Wijland³

¹*Center for Soft Condensed Matter Physics and Interdisciplinary Research & School of Physical
Science and Technology, Soochow University, 215006 Suzhou, China*

²*School of Physics and Astronomy and Institute of Natural Sciences, Shanghai Jiao Tong Univer-
sity, Shanghai 200240, China*

³*Université Paris Cité, Laboratoire Matière et Systèmes Complexes (MSC), UMR 7057 CNRS,
F-75205 Paris, France*

⁴*Department of Physics, Technion – Israel Institute of Technology, Haifa 3200003, Israel*

⁵*Department of Physics, Massachusetts Institute of Technology, Cambridge, Massachusetts 02139,
USA*

† Corresponding authors: yfzhao2021@suda.edu.cn

June 3, 2024

**The Young-Dupré equation is a cornerstone of the equilibrium theory of capillary and wet-
ting phenomena. In the biological world, interfacial phenomena are ubiquitous, from the
spreading of bacterial colonies to tissue growth and flocking of birds, but the description of
such active systems escapes the realm of equilibrium physics. Here we show how a micro-**

scopic, mechanical definition of surface tension allows us to build an Active Young-Dupré equation able to account for the partial wetting observed in simulations of active particles interacting via pairwise forces. Remarkably, the equation shows that the corresponding steady interfaces do not result from a simple balance between the surface tensions at play but instead emerge from a complex feedback mechanism. The interfaces are indeed stabilized by a drag force due to the emergence of steady currents, which are themselves a by-product of the symmetry breaking induced by the interfaces. These currents also lead to new physics by selecting the sizes and shapes of adsorbed droplets, breaking the equilibrium scale-free nature of the problem. Finally, we demonstrate a spectacular consequence of the negative value of the liquid-gas surface tensions in systems undergoing motility-induced phase separation: partially-immersed objects are expelled from the liquid phase, in stark contrast with what is observed in passive systems. All in all, our results lay the foundations for a theory of wetting in active systems.

1 Introduction

The Young-Dupré equation describes the equilibrium wetting of a macroscopic liquid droplet on a solid surface as illustrated in Fig. 1. It determines the contact angle φ between the liquid-gas interface and the solid surface through

$$\gamma_{GS} - \gamma_{LS} = \gamma_{LG} \cos \varphi, \quad (1)$$

where γ_{XY} is the surface tension between phases X and Y . This equation is a cornerstone of the theory of capillary phenomena ¹, with implications ranging from wetting transitions ² to finite

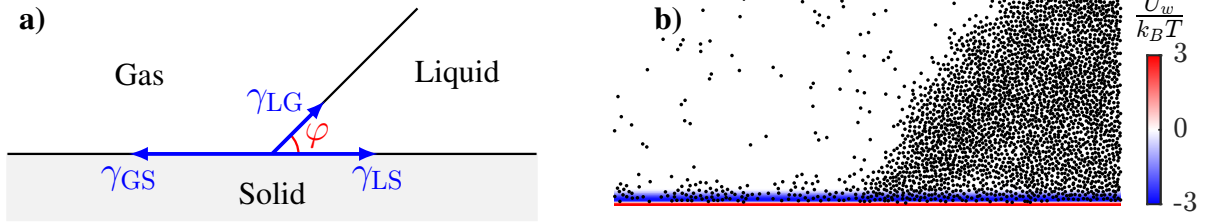


Figure 1: **a)** In equilibrium, when a macroscopic droplet wets a solid surface, the contact angle φ satisfies the Young-Dupré equation (1). **b)** Snapshot of a phase-separating passive system partially wetting of a solid confining wall. At the particle scale, the liquid-gas interface is an elusive object. Nevertheless, the Young-Dupré equation endows this interface with mechanical properties at the macroscopic scale: in this picture, the arrows in panel a) define the directions of the macroscopic forces exerted on the contact line for positive surface tensions. See methods for numerical details. relaxation times in liquid entrainment ^{3,4}. A remarkable property of the Young-Dupré equation is that it endows interfaces, which are macroscopic objects, with mechanical properties: Eq. (1) can be read as a force-balance condition along the direction tangential to the solid substrate, even though interfaces are elusive objects at the particle scale where the forces are actually exerted. In equilibrium, an important challenge has thus been to bridge these macroscopic ‘forces’ to their microscopic origin, which results from the interplay between particle interactions and thermal fluctuations ⁵. Meeting this challenge has led to a comprehensive understanding of interface physics in equilibrium ⁶⁻⁸.

Reaching a comparable state of understanding in active matter is an important open challenge due to the flurry of interfacial phenomena observed in active systems—from the growth of cellular tissues ⁹ and bacterial colonies ¹⁰ to the cohesion of flocks of birds ¹¹ or colloidal rollers ¹². The

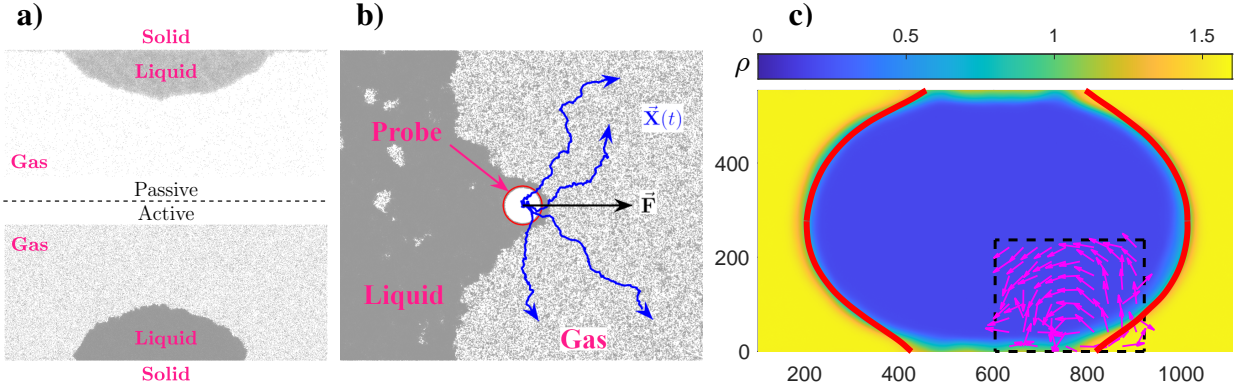


Figure 2: **(a)** Snapshots of passive (top) and active (bottom) droplets wetting solid surfaces, showing the apparent similarities between the two cases. Throughout the article, grey dots indicate the particle positions. **(b)** Wilhelmy-plate setup. A circular plate (red) is first pulled out of a liquid phase and then held fixed while the system relaxes. In the steady state, the liquid bulk is connected to the plate through a capillary bridge. The plate is then released and moves according to Hamiltonian dynamics due to its interaction with the active particles. Four representative plate trajectories are shown in blue, which all show the expulsion of the plate, at odd with the equilibrium case in which the plate would be pulled inside the liquid phase due to the positive liquid-gas surface tension. See SM Movie 1 for a representative realization. **(c)** Phase-separated system comprising Active Brownian Particles, with periodic boundary conditions along \hat{x} and confining walls at the bottom and top of the system. Color encodes the density $\rho(\mathbf{r})$. The red curves shows the prediction of the liquid-gas interface from the active Young-Dupré equation. The measurements of the surface tensions detailed in Methods give $\gamma_{LS} = -1708 \pm 30$, $\gamma_{GS} = -2255 \pm 15$, and $\gamma_{LG} = -192 \pm 3$, so that $|\gamma_{LS} - \gamma_{GS}| > \gamma_{LG}$, which demonstrates the failure of the standard Young-Dupré equation (1). In the region delimited by the black dashed line, we show the particle flow \mathbf{J} that emerges close to the triple point.

quest for a micro-to-macro theory of interface dynamics in active systems has thus attracted an upsurge of attention over the past few years ^{13–31}. So far, however, a comprehensive theory of interface mechanics and equilibria is lacking for active systems, which raises the question as to whether a counterpart to the Young-Dupré equation exists in this context. Filling this gap is the goal of this article.

An inspiring and fruitful starting point consists in directly exporting equilibrium results and methodology to active materials. However, an important difficulty arises from the continuous injection of energy and momentum in the steady state of active systems, which endows them with anomalous mechanical properties ³². For instance, it was recently argued that the drag forces that accompany steady-state currents may impact the mechanical balance ³³, an effect whose consequences have not been explored so far. Another difficulty in addressing the fate of the Young-Dupré equation is the need to measure all involved surface tensions. To do so, one requires a working definition of γ_{GS} , γ_{LS} , and γ_{LG} . While fluid-solid surface tensions have been defined recently ³³, the liquid-gas surface tension has been the topic of much controversy ^{14,21,30,34,35}. Progress has been made on this question by considering the workhorse models of self-propelled particles interacting via pairwise forces ³⁶. These systems undergo a Motility-Induced Phase Separation (MIPS) between a dilute and a dense phase in the presence of repulsive forces at large enough density and propulsion speed ^{36–38}. As illustrated in Fig. 2a, partial wetting is observed in the presence of a confining solid surface, similarly to what is observed for a passive liquid droplet. (All our simulations are detailed in Methods.) For such models, an interesting inroad into surface tension was recently proposed ¹⁴ by assuming that the equilibrium expression of a liquid-gas surface tension ^{6,39,40} also

holds for active interfaces:

$$\gamma_{\text{LG}} = \int_{\mathbf{r}_G}^{\mathbf{r}_L} dr_{\perp} [p_{\perp} - p_{\parallel}(r_{\perp})], \quad (2)$$

where \mathbf{r}_G and \mathbf{r}_L are positions in the bulk gas and liquid phases, respectively, and r_{\perp} is a coordinate normal to the interface. In Eq. (2), p_{\perp} is the pressure normal to the interface while $p_{\parallel}(x)$ is the tangential pressure. An appealing feature of this definition is that, as in equilibrium, it has been shown to control the finite-size corrections to coexisting densities of liquid and gas droplets⁴¹. However, Eq. (2) has also been challenged for a number of reasons^{21,30,34,35}, starting from its negative sign that, in passive systems, signals an unstable interface. Furthermore, a *direct* measurement of the force induced by the surface tension, as defined in Eq. (2), is lacking. This has left room for alternative definitions of γ_{LG} that result in a positive value^{21,30,34}.

To settle this debate, we first derive Eq. (2) from first principles and show that the resulting γ_{LG} is indeed a measurable force exerted along interfaces, and that it is negative. A remarkable consequence of this is illustrated in Fig. 2b using a numerical simulation inspired by the Wilhelmy-plate experiment. At odds with the equilibrium phenomenology, in which a plate partially immersed in the liquid phase is pulled into the liquid due to the positive surface tension, our plate is *expelled* from the active liquid phase.

This validation of Eq. (2) as a *bona fide* liquid-gas surface tension however comes with a challenge: In the stable partial wetting situation shown in Fig. 2a, all surface tensions can now be measured, but they lead to violations of the Young-Dupré equation (1). Indeed, we measure (see

SM):

$$|\gamma_{GS} - \gamma_{LS}| > \gamma_{LG} , \quad (3)$$

which should lead to a complete dewetting according to Eq. (1). The competition between the surface tensions alone is thus unable to stabilize partial wetting. As we show below, the important missing link in Eq. (2) are the drag forces emerging from steady currents, which play a central role in reaching force balance. In the semi-infinite setting described in Fig. 1, we derive the active Young-Dupré equation which reads,

$$\gamma_{GS} - \gamma_{LS} = \gamma_{LG} \cos \varphi + F_D \quad (4)$$

with F_D the total drag force experienced by the particles. Along with the mechanical interpretation of the negative surface tension, this is the central result of this article.

As its equilibrium counterpart, our Active-Young-Dupré equation has to be modified in finite systems, due to Laplace-pressure corrections induced by the finite curvature of interfaces. This modified equation can then be used to predict the full shape of the liquid-gas interface, as shown by the red curve in Fig. 2c. This quantitative description of the interface requires accounting for the steady vortex current generated in the vicinity of the triple point. Since the solid wall is invariant by translation, the existence of these currents stems from the spontaneous breaking of this symmetry induced by the emerging interface, which is in turn stabilized by the currents it generates: the stability of partial wetting is an emergent phenomenon in our active system.

Finally, we close this article by reporting a spectacular consequence of the role played by steady currents: while the selection of the contact angle is a scale-free problem in passive systems,

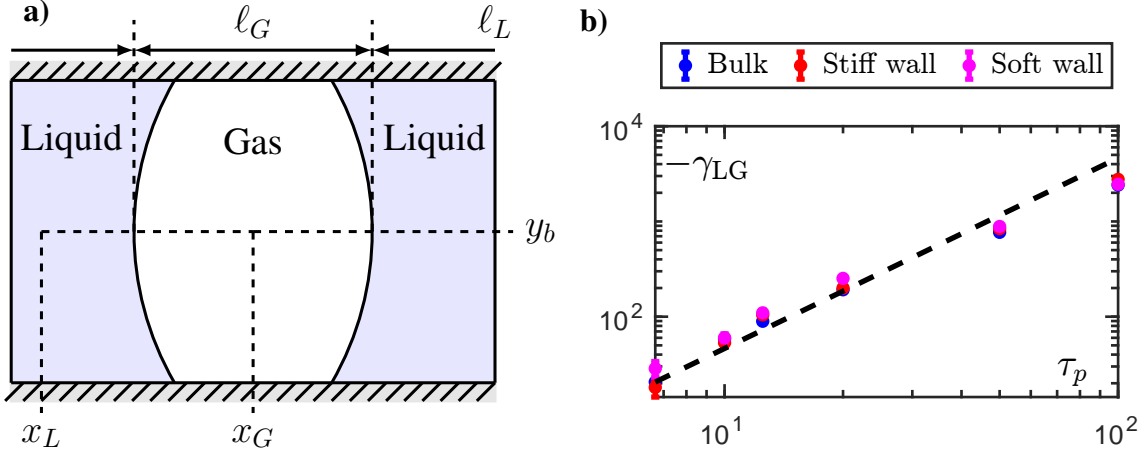


Figure 3: **(a)** The setup used to measure the liquid-gas surface tension γ_{LG} . **(b)** The measurements of γ_{LG} from the wall force through Eq. (11) (red and magenta symbols) and its bulk counterpart Eq. (10) (blue symbols), agree quantitatively for persistence times ranging from $\tau_p = 5$ to $\tau_p = 100$. Equation (10) suggests that γ_{LG} should scale as the active stress tensor, $\sigma^a \propto v_0^2 \tau_p$, multiplied by the width of the interface region, $v_0 \tau_p$. The overall scaling $\gamma_{LG} \propto \tau_p^2$ is confirmed by the dashed black line.

independent of the size R of an adsorbed droplet at all scales above the particle size, this is no longer true in active systems. Instead, the large-scale vortex flow generated at the triple point prevents the existence of macroscopic droplets and arrest the growth of the droplet as the density of the system increases, leading instead to a complex intermittent dynamics involving splitting and merging of finite droplets illustrated in SM Movie 2.

2 Surface (ex)tension: when interfaces push on confining walls.

We consider systems in which the particle propulsion forces have an autonomous dynamics, which warrants the existence of an equation of state for the pressure ⁴². These systems include standard active dynamics like run-and-tumble ⁴³, active Brownian ³⁶ or active Ornstein-Uhlenbeck ^{9,44} models in the presence of pairwise forces between the particles. For the sake of concreteness, we work with overdamped active Brownian particles (ABPs) in two dimensions interacting through short-range pairwise repulsive forces, but our results apply in $d \geq 2$ dimensions to all models pertaining to this broader class. The equations of motion for particle i at position \mathbf{r}_i and orientation angle θ_i read:

$$\dot{\mathbf{r}}_i = v_0 \mathbf{u}(\theta_i) - \mu \sum_{j \neq i} \nabla_{\mathbf{r}_i} U(\mathbf{r}_i - \mathbf{r}_j) - \mu \nabla_{\mathbf{r}_i} U_w(\mathbf{r}_i), \quad (5)$$

$$\dot{\theta}_i = \sqrt{2/\tau_p} \xi_i, \quad (6)$$

where v_0 is the particle propulsion speed, μ their mobility, τ_p the persistence time, and $\mathbf{u}(\theta) = (\cos \theta, \sin \theta)$. In our simulations, the particles interact via a harmonic repulsive potential $U(\mathbf{r}) = \epsilon(r - r_0)^2 \Theta(r - r_0)$, with $r = |\mathbf{r}|$, r_0 the diameter of the particles, and $\Theta(r)$ the Heaviside step function. When the system is in presence of a confining solid boundary, we model the latter as a repulsive potential $U_w(\mathbf{r})$, following the seminal work of Navascués and Berry ⁴⁰. The centered Gaussian white noises ξ_i satisfy $\langle \xi_i(t) \xi_j(t') \rangle = \delta_{ij} \delta(t - t')$, where the brackets represent averages over noise realizations.

The sole hydrodynamic field of this model is the density $\rho(\mathbf{r}, t) = \langle \sum_i \delta[\mathbf{r} - \mathbf{r}_i(t)] \rangle$, whose

dynamics is given by a local conservation law^{32,41,45}:

$$\dot{\rho} = -\nabla \cdot \mathbf{J}; \quad \mathbf{J} = \mu[\nabla \cdot \boldsymbol{\sigma} - \rho \nabla_{\mathbf{r}} U_w(\mathbf{r})], \quad (7)$$

where $\mathbf{J}(\mathbf{r}) = \langle \sum_i \dot{\mathbf{r}}_i \delta(\mathbf{r} - \mathbf{r}_i(t)) \rangle$ is the particle current (See SM). In Eq. (7), $\boldsymbol{\sigma}$ acquires the physical meaning of a stress tensor in the steady state. It then comprises two contributions^{45–48}: $\boldsymbol{\sigma} = \boldsymbol{\sigma}^{\text{IK}} + \boldsymbol{\sigma}^{\text{a}}$, with $\boldsymbol{\sigma}^{\text{IK}}$ the standard Irving-Kirkwood contribution stemming from the pairwise interactions between the particles and $\boldsymbol{\sigma}^{\text{a}}$ a contribution due to the active forces. Equation (7) is well established^{41,45,49–51} and it is the starting point of our theory.

Consider a phase-separated system in the presence of periodic boundary conditions along \hat{x} , confined along the \hat{y} direction by two walls at the top and bottom of the system (see Fig. 3). Using this setting, we now relate the definition (2) of surface tension to an actual force measurement starting from the microscopic dynamics (5)-(6). The force density on the upper wall can be measured as $f_w(x) = \int_{y_b}^{\infty} dy \rho(x, y) \partial_y U_w(y)$, where y_b is a position deep in the bulk of the system, far away from the walls. In the liquid and gas phases, the system exerts an upward force per unit length on the upper wall equal to the bulk pressures, given by p_L and p_G , respectively¹.

To extract the contributions of the liquid-gas interfaces to the total force exerted on the upper wall, $F_{w,\text{tot}} = \int_0^{L_x} dx' f_w(x')$, we use Eq. (7) to integrate $J_y \equiv \mathbf{J} \cdot \hat{y}$ over the upper half of the system, for $y > y_b$ and $0 \leq x \leq L_x$. This leads to

$$F_{w,\text{tot}} = - \int_0^{L_x} dx' \sigma_{yy}(x', y_b) - \int_{y \geq y_b} d^2 \mathbf{r} \frac{J_y}{\mu}, \quad (8)$$

¹Note that p_G and p_L need not be equal due to the curved interface separating the gas and liquid phases.

where we have used that $\sigma_{xy} = 0$ away from the interfaces since the bulk liquid and gas phases are locally isotropic. In the steady-state, $\nabla \cdot \mathbf{J} = 0$ implies that the integral of J_y vanishes. We then note that $-\int_0^{L_x} dx' \sigma_{xx}(x', y_b) = \ell_G p_G + \ell_L p_L$, where $\ell_{G/L}$ are the total lengths of the gas and liquid phases, respectively. Adding and subtracting this contribution to Eq. (8) then leads to

$$F_{w,\text{tot}} = -n_{\text{LG}}\gamma_{\text{LG}} + \ell_G p_G + \ell_L p_L, \quad (9)$$

where n_{LG} is the number of liquid-gas interfaces and we identify the liquid-gas surface tension γ_{LG} as

$$\gamma_{\text{LG}} = \int_{x_L}^{x_G} dx [\sigma_{yy}(x, y_b) - \sigma_{xx}(x, y_b)]. \quad (10)$$

Equation (10) is equivalent to the one proposed in Eq. (2), upon the identification $p_{\parallel}(x, y) = -\sigma_{xx}(x, y)$ and $p_{\perp} = -\sigma_{yy}(x, y)$ ^{21,41,52,53}. It allows one to measure γ_{LG} far away from the confining walls and it predicts that the surface tension obeys an equation of state. This bulk, stress-tensor based definition of γ_{LG} can now be given a proper mechanical definition as a force thanks to Eq. (9):

$$\gamma_{\text{LG}} = -\frac{1}{n_{\text{LG}}} [F_{w,\text{tot}} - p_L \ell_L - p_G \ell_G]. \quad (11)$$

Equation (11) matches our equilibrium intuition that surface tension is the contribution to the force exerted on the upper wall due to the presence of interfaces. As shown in Fig. 3, Eqs. (10) and (11) quantitatively agree in our simulations over a wide range of persistence lengths, independently of the choice of the wall potential. The *negative* value of the surface tension is confirmed: the interface exerts a repulsive, outward force on the upper and bottom walls, in striking contrast with the equilibrium case.

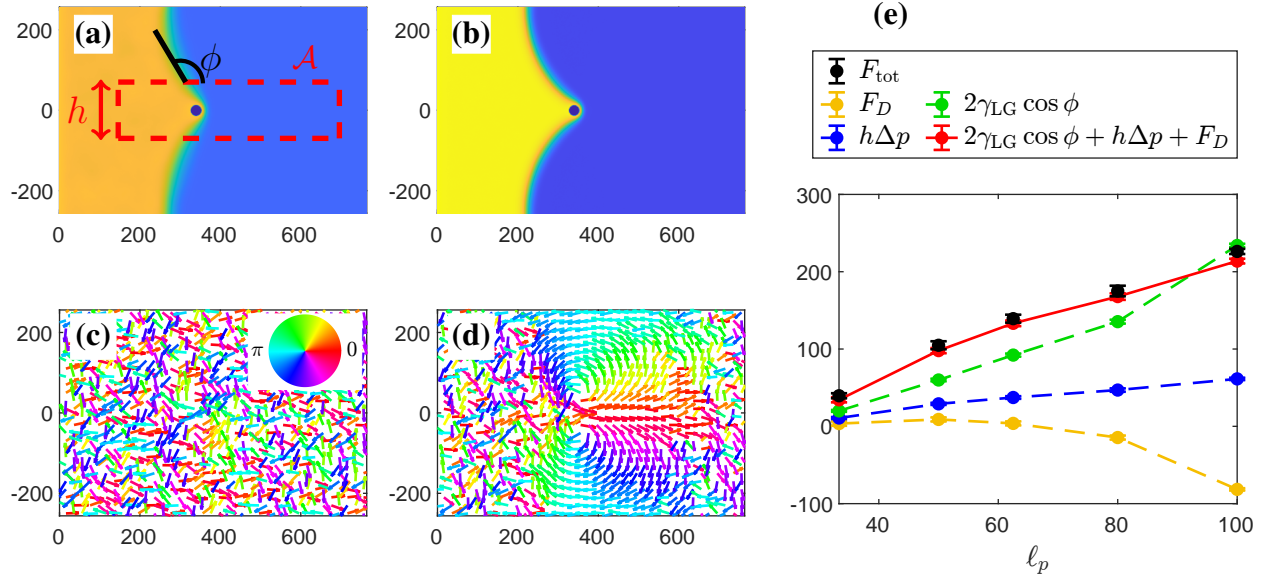


Figure 4: Forces exerted on Wilhelmy plates. **(a-b)** Density fields of active particles with $\tau_p = \frac{20}{3}$ (a) and $\tau_p = 50$ (b), speed $v_0 = 5$ and plate radius $R_p = 16$. The color code is the same as in Fig. 2c. **(c-d)** The current fields corresponding to (a) and (b), respectively. The arrow lengths are proportional to $\log |\mathbf{J}/10^{-6}|$ and their color encodes the current direction. **(e)** The various contributions to the total force F_{tot} on the plate, as a function of ℓ_p .

3 The Wilhelmy plate experiment

The mechanical consequence of the negative liquid-gas surface tension can be evidenced using a setup inspired by the Wilhelmy plate experiment^{54,55}. In the latter, a plate—or a ring in a variant introduced by Pockels and du Noüy⁵⁶—is inserted into a liquid-gas interface and slowly pulled out of the liquid. In equilibrium, the positive surface tension γ_{LG} then exerts a restoring force on the plate, pulling it into the liquid and resisting the outward motion. The measurement of the force on the plate can then be used to extract γ_{LG} ⁵⁷.

Figure 2b shows a similar experiment carried out with a disk immersed in the vicinity of the liquid-gas interface. As in the Wilhelmy-plate experiment, a capillary bridge forms, leading to a deformation of the interface. In our active bath, we then expect surface tension to induce a net force on the plate, and the negative value of γ_{LG} to translate into an *outward* force. To test this, we release our ‘plate’ at the configuration shown in Fig. 2b, and let its position \mathbf{r}_p evolve according to:

$$M\ddot{\mathbf{r}}_p = - \sum_i \nabla_{\mathbf{r}_p} U_w(\mathbf{r}_p - \mathbf{r}_i), \quad (12)$$

where M is the mass of the plate and $U_w(\mathbf{r})$ now describes the interaction potential between the plate and the active particles. Four representative trajectories are displayed in Fig. 2b, which all show the *expulsion* of the plate out of the liquid phase, in stark contrast with the passive case. As we now show, the force on the plate can be connected to the liquid-gas surface tension γ_{LG} . However, an important difference with the passive setting is that, here, emergent steady currents play a major role in the plate dynamics.

To proceed, we integrate Eq. (7) over a region $\mathcal{A} = [x_G, x_L] \times [-h/2, h/2]$ that encompasses the disk, with $x_{G,L}$ abscissa deep in the gas and liquid phases, respectively (See Fig. 4a), leading to

$$F_{\text{tot}} = \int_{\mathcal{A}} (\partial_x \sigma_{xx} + \partial_y \sigma_{xy}) d^2 \mathbf{r} + F_D; \quad (13)$$

where F_{tot} is the average total force exerted by the fluid on the disk along \hat{x} and

$$F_D = - \int_{\mathcal{A}} \frac{J_x}{\mu} d^2 \mathbf{r} = \sum_{i|\mathbf{r}_i \in \mathcal{A}} -\frac{1}{\mu} \langle \dot{\mathbf{r}}_i \rangle \quad (14)$$

is the total drag exerted on the particles contained in the region \mathcal{A} . Since σ_{xy} vanishes in bulk phases, the integral of $\partial_y \sigma_{xy}$ in Eq. (13) picks a contribution only from the interface, which is equal to $\gamma_{LG} \cos \phi$ (see SM), where ϕ is the angle between the interface and the \hat{x} axis (see Fig. 4a). All in all, the average total force exerted on the probe is given by

$$F_{\text{tot}} = 2\gamma_{LG} \cos \phi + h\Delta p + F_D, \quad (15)$$

where $\Delta p = p_L - p_G$ is the pressure jump between the liquid and gas phases due to the curved interface⁴¹. Independent measurements of the contributions entering Eq. (15) are shown in Fig. 4e, for a plate held fixed, together with maps of the average density and current fields for two different persistence lengths. These measurements confirm the prediction (15), within a few percent.

As predicted, the surface-tension contribution, $2\gamma_{LG} \cos \phi$, pushes the plate towards the gas phase. As we show in SM, Δp has contributions not only from an equilibrium-like Laplace term but also from steady-state currents. Figure 4 shows that the overall (small) contribution of Δp is also to expel the plate from the liquid. Finally, for short persistence lengths, the currents are negligible (Fig. 4c) and barely contribute to the force on the plate. On the contrary, at large persistence

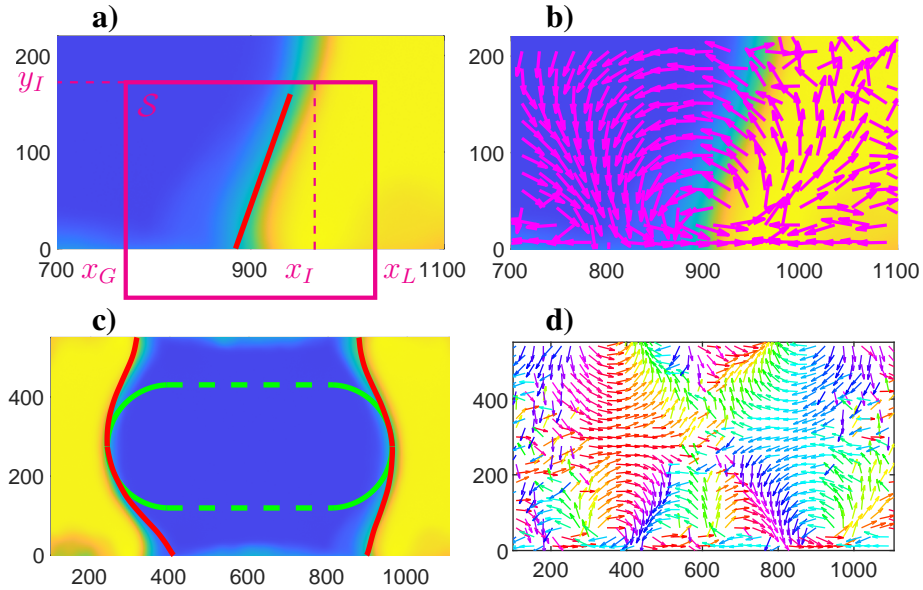


Figure 5: The active Young-Dupré Equation. **(a)** The density field in the vicinity of the tripple point. The red line shows the prediction of the angle given by Eq. (16) as $y_I \rightarrow 0$. **(b)** The current field corresponding to Panel (a). **(c) - (d)** show the full coexistence region for the same system as (a)-(b). The red curves show the interface predicted by Eq. (17), while the green curve shows the current-free prediction, setting $F_D = 0$. Finite wetting is only possible thanks to the stabilizing effect of the vortex flow. The arrow lengths in panels (b) and (d) are proportional to $\log |\mathbf{J}/10^{-6}|$. The color in panel (d) encodes the current direction, as in Fig. 4c.

lengths, large-scale vortices develop in the vicinity of the plate (Fig. 4d). Interestingly, they oppose the interface contribution and tend to push the plate back into the liquid. All in all, the expulsion of the plate by the fluid is an unambiguous demonstration that the surface tension of active fluids, understood in its traditional mechanical sense, is indeed negative.

4 The active Young-Dupré equation

Now that the mechanical interpretation of γ_{LG} has been firmly established, let us turn back to the phase-separated system introduced in Fig. 2 and show how the surface tensions enter the force balance at the triple point. In Fig. 5, we show the same situation with a softer wall, which leads to a larger contact angle. To account for this variation, we derive the active Young-Dupré Eq. (16). To do so, we integrate the projection of Eq. (7) along \hat{x} over the region \mathcal{S} shown in Fig. 5a, which encompasses the liquid-gas interface up to a height y_I . This leads to

$$0 = \gamma_{LS} - \gamma_{GS} - y_I \Delta p + \gamma_{LG} \cos \phi(y_I) + F_D(y_I), \quad (16)$$

where the fluid-solid surface tensions are defined as ³³ $\gamma_{GS,LS} = y_I p_{G,L} + \int_{-\infty}^{y_I} dx \sigma_{xx}(x_{G/L}, y)$, $\phi(y_I)$ is the angle between the liquid-gas interface and the horizontal axis at the interface coordinate x_I, y_I , and F_D is the total drag exerted on the particles in the region \mathcal{S} . We note that, contrary to the case depicted in Fig. 1 for which the Young-Dupré's law is typically derived, the liquid-gas interface is curved in our simulations, leading in general to a non-zero $\Delta p = p_L - p_G$; Such a term would also be present for a passive system.

We now use the simulations shown in Fig. 5 to test the prediction for the contact angle φ .

To do so, we need to evaluate each term entering Eq. (16). The surface tensions can be evaluated in the bulk of the system, where they are independent of y_I . Then, a natural definition of the contact angle amounts to take the limit of $\phi(y_I)$ as $y_I \rightarrow 0$. In this limit, the contribution of the pressure difference vanishes and we recover Eq. (4). Fig. 5a compares the prediction of the active Young-Dupré equation with the liquid-gas interface measured in numerical simulations. Despite evaluating the surface tension in the bulk of the system, the agreement between measured and predicted contact angles are very good. As expected, the macroscopic contact angle describes the behaviour of the smoothly varying interface at $y \geq \ell_p$ as it approaches the lower, and it does not resolve the microscopic structure on the scale $y < \ell_p$. (See SM Fig S6 for similar measurements for other persistence times and wall stiffnesses.) We stress that partial wetting, leading to a finite contact angle, is only possible thanks to the strong vortex flow created at the triple point, shown in Fig. 5b.

Note that the active Young-Dupré equation can be used to predict not only the contact angle but also the full shape of the interface by writing that $\cot \phi(y_I) = x'_I(y_I)$. Equation (16) can then be turned into a differential equation for $x_I(y_I)$, whose solution reads

$$x_I(y_I) - x_I(L_y/2) = \int_{L_y/2}^{y_I} dy \frac{\gamma_{LS} - \gamma_{GS} + F_D(y) - y\Delta p}{\sqrt{\gamma_{LG}^2 - [\gamma_{LS} - \gamma_{GS} + F_D(y) - y\Delta p]^2}}. \quad (17)$$

The predictions of Eq. (17) are shown as red curves in Fig. 5c, and compare well with the interface measured in the simulations. The Active Young-Dupré equation can thus be used to account for the full interface shape.

We stress that, in all the cases that we have studied, steady currents are instrumental in

achieving the mechanical balance. Indeed, solving Eq. (17) for $F_D = 0$ predicts a circular shape of radius $\gamma_{LG}/\Delta p$, which is shown in green in Fig. 5c. In all our simulations, this current-free solution systematically fails to describe the interface. Partial wetting is thus only possible in this system thanks to the presence of steady-state currents. The physical origin of these currents relies on a subtle feedback mechanism: they are not externally imposed by the confining walls, which are invariant by translation along \hat{x} ; Instead, they result from a spontaneous symmetry breaking due to the liquid-gas interface, which is itself stable only thanks to the current it generates.

5 Droplet instability and intermittent dynamics

In equilibrium, the solution of the passive Young-Dupré equation—including its correction due to Laplace pressure—is a circular segment with a fixed contact angle such that $\cos \varphi_{\text{eq}} = \frac{\gamma_{GS} - \gamma_{LS}}{\gamma_{LG}}$ (Fig. 6a). Increasing the average density then leads to droplets of increasing radii at fixed contact angles φ_{eq} , that can all be collapsed onto a master curve by dividing the interface coordinate x_I, y_I by the droplet height h : The system admits static scale-free solutions Fig. 6b.

In the active case, the active Young-Dupré equation also includes the drag force, and the Laplace pressure is dressed by currents (See SM). Since the current field is a complex, non-local functional of the full system configuration, droplets of increasing sizes lead to different values of F_D , so that the contact angle cannot be independent of the droplet size. In particular, a macroscopic droplet requires a vanishing radius of curvature, leading to a locally straight interface, as depicted in Fig. 1a. This requires an angle $\phi(y_b)$ independent of y_b , which is in direct contradiction with

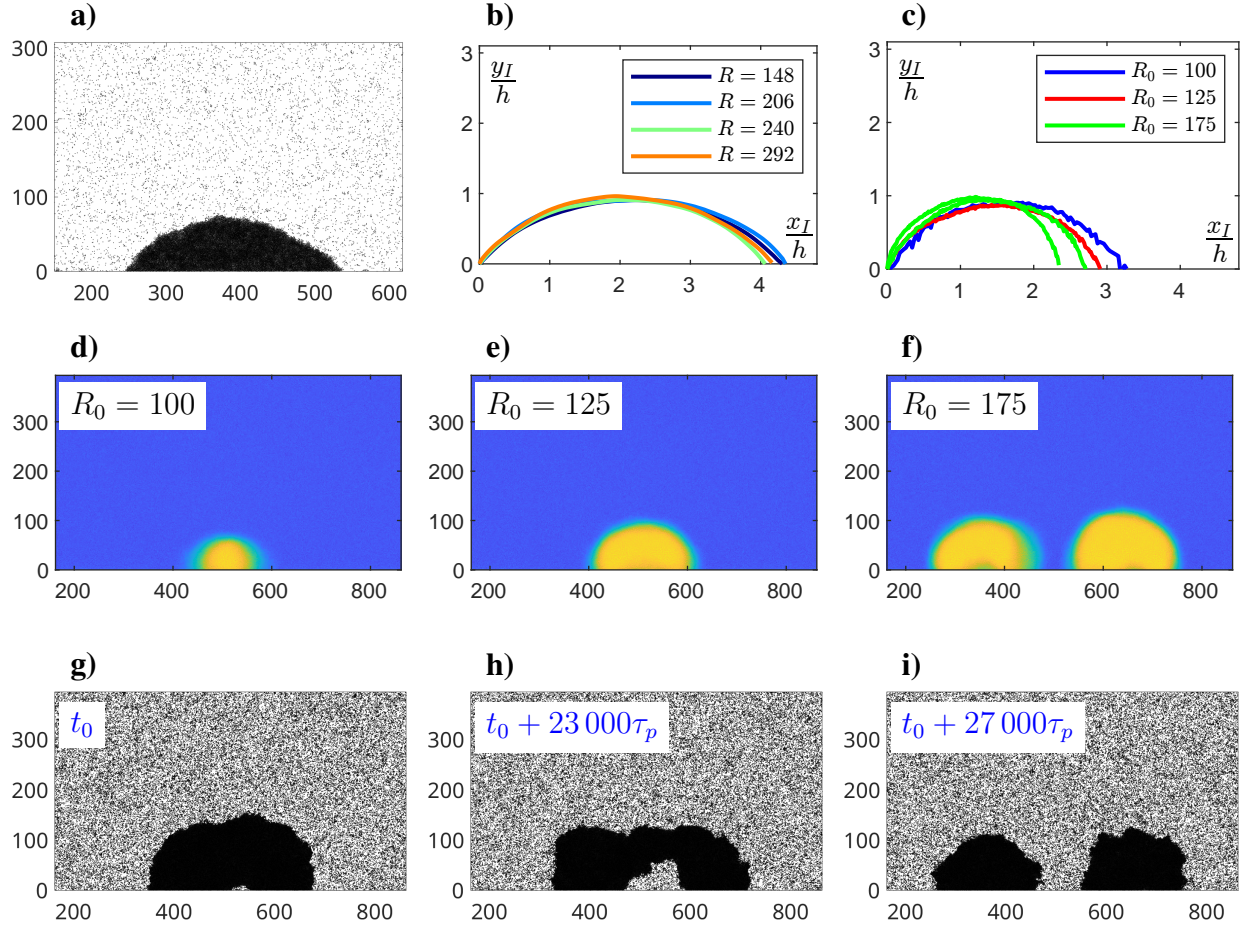


Figure 6: Size-selection and intermittent dynamics of active droplets adsorbed on a wall. **(a-b)** Passive droplets have a size-independent contact angle. A snapshot is shown in panel (a) while panel (b) shows the average interfaces, upon rescaling x and y by the droplets heights. This demonstrates the scale-free nature of the droplet in the passive case. **(c-f)** Average active-droplet shape as their initial radii R_0 increase. Panel (d-f) show the average density profile of the droplets using the color code of Fig. 2c. Large values of R_0 leads to the splitting of the initial droplet. Panel (c) show the lack of scale-free nature of the active system: the current field generated by the droplet are size-dependent, hence selecting acceptable values of (φ, R) . Unlike in the passive case, large droplets are unstable and split, leading to a rich dynamics illustrated in the successive snapshots shown in panels g-i and in SI Movie 2.

the fact that $F_D(y_b)$ varies with y_b . As such, we expect the active Young-Dupré equation to forbid macroscopic active droplets.

To test this, we simulated droplets of increasing sizes and report their average density profiles and interfaces on Fig. 6d-f and Fig. 6c, respectively. As the density increases, not only do the average profiles vary, but large droplets break into smaller ones (Fig 6f). First, the drag force selects admissible droplet sizes, hence breaking the scale-free nature of the passive system. Then, like any object embedded in an active fluid, the droplets have complex interactions, mediated by the particles currents⁵⁸⁻⁶⁴. The result is a rich intermittent dynamics with many merging and splitting events illustrated in Fig. 6g-i and in SM Movie 2. Note that, on the contrary, the phase-separated profiles shown in Fig. 5 are all stable over time. As the density increases, the transition between the droplets shown in Fig. 6 and these macroscopic phase-separated profiles is thus likely to involve complex structures that are certainly worthy of further exploration.

6 Conclusion.

In this article, we have demonstrated that the liquid-gas surface tension γ_{LG} of an active fluid undergoing motility-induced phase separation can be defined in terms of a force measurement, starting from the microscopic particle dynamics, and that it is negative. We have shown this mechanical definition to agree with the bulk definition in terms of stress-tensor anisotropy suggested in⁶⁵, which shows that γ_{LG} is a state variable. A spectacular illustration of this negative surface tension is the expulsion of a partially-immersed plate from the liquid phase, at odds with what

happens in the Wilhelmy-plate experiment for passive systems.

As in equilibrium, this mechanical definition of surface tension also plays a thermodynamic role in controlling the contact angle at a triple point. However, the breaking of parity symmetry in the vicinity of the triple point leads to the emergence of large vortices of steady-state particle currents. In turn, these currents lead to a steady drag that impacts the mechanical balance, leading to a new Active Young-Dupré equation. The latter shows that the steady currents are the key players that make the existence of the partial wetting of purely repulsive walls possible. They also lead to new physics: their large-scale structure and their non-local dependence on the system configuration indeed prevents the existence of scale-free droplet solutions, leading instead to a rich dynamics with intermittent merging and splitting events.

All in all, we hope that this work will contribute to the ongoing effort to understand and control the physics of interfaces in active systems. Many open questions now lie ahead of us, from the size-selection mechanism of adsorbed droplets to the generalization of our Active Young-Dupré equation to systems coupled to momentum-conserving fluids. Partial wetting is observed in many experimental synthetic ⁶⁶ and biological ^{26,28,67-71} active systems. A complete theory of active wetting for these systems will likely require to investigate situations in which pressure and surface tensions also include equation-of-state violating contributions ^{32,72}, which remain uncharted territory at this stage. We hope that the methods introduced in this article will prove instrumental to tackle these challenging cases.

7 Acknowledgments

FvW, JT & RZ thank K. Mandadapu at UC Berkeley for hospitality and discussions, YZ acknowledges support from National Natural Science Foundation of China (Grant 12304252), YK acknowledges financial support from ISF (2038/21) and NSF/BSF (2022605). FvW and JT acknowledge support from ANR Thema.

References and Notes

1. De Gennes, P.-G. Wetting: statics and dynamics. *Reviews of modern physics* **57**, 827 (1985).
2. Bonn, D., Eggers, J., Indekeu, J., Meunier, J. & Rolley, E. Wetting and spreading. *Rev. Mod. Phys.* **81**, 739–805 (2009).
3. Snoeijer, J. H., Delon, G., Fermigier, M. & Andreotti, B. Avoided critical behavior in dynamically forced wetting. *Physical review letters* **96**, 174504 (2006).
4. Bertrand, E., Blake, T. & De Coninck, J. Dynamics of dewetting. *Colloids and Surfaces A: Physicochemical and Engineering Aspects* **369**, 141–147 (2010).
5. Tarazona, P. & Navascués, G. A statistical mechanical theory for line tension. *The Journal of Chemical Physics* **75**, 3114–3120 (1981). URL <https://doi.org/10.1063/1.442366>.
6. Rowlinson, J. & Widom, B. Molecular theory of capillarity 1982. *Clarendon: Oxford* 56 (1982).

7. Marchand, A., Weijs, J. H., Snoeijer, J. H. & Andreotti, B. Why is surface tension a force parallel to the interface? *American Journal of Physics* **79**, 999–1008 (2011). URL <http://aapt.scitation.org/doi/10.1119/1.3619866>.
8. De Gennes, P.-G., Brochard-Wyart, F. & Quéré, D. *Capillarity and wetting phenomena: drops, bubbles, pearls, waves* (Springer Science & Business Media, 2013).
9. Sepúlveda, N. *et al.* Collective cell motion in an epithelial sheet can be quantitatively described by a stochastic interacting particle model. *PLoS computational biology* **9**, e1002944 (2013).
10. Hallatschek, O., Hersen, P., Ramanathan, S. & Nelson, D. R. Genetic drift at expanding frontiers promotes gene segregation. *Proceedings of the National Academy of Sciences* **104**, 19926–19930 (2007).
11. Bialek, W. *et al.* Statistical mechanics for natural flocks of birds. *Proceedings of the National Academy of Sciences* **109**, 4786–4791 (2012).
12. Bricard, A., Caussin, J.-B., Desreumaux, N., Dauchot, O. & Bartolo, D. Emergence of macroscopic directed motion in populations of motile colloids. *Nature* **503**, 95–98 (2013).
13. Joanny, J.-F. & Ramaswamy, S. A drop of active matter. *Journal of fluid mechanics* **705**, 46–57 (2012).
14. Bialké, J., Siebert, J. T., Löwen, H. & Speck, T. Negative interfacial tension in phase-separated active brownian particles. *Phys. Rev. Lett.* **115**, 098301 (2015). URL <https://link.aps.org/doi/10.1103/PhysRevLett.115.098301>.

15. Speck, T. Stochastic thermodynamics for active matter. *Europhysics Letters* **114**, 30006 (2016).
16. Marconi, U. M. B., Maggi, C. & Melchionna, S. Pressure and surface tension of an active simple liquid: a comparison between kinetic, mechanical and free-energy based approaches. *Soft Matter* **12**, 5727–5738 (2016).
17. Paliwal, S., Prymidis, V., Filion, L. & Dijkstra, M. Non-equilibrium surface tension of the vapour-liquid interface of active Lennard-Jones particles. *The Journal of chemical physics* **147**, 084902 (2017).
18. Patch, A., Sussman, D. M., Yllanes, D. & Marchetti, M. C. Curvature-dependent tension and tangential flows at the interface of motility-induced phases. *Soft matter* **14**, 7435–7445 (2018).
19. Tjhung, E., Nardini, C. & Cates, M. E. Cluster phases and bubbly phase separation in active fluids: reversal of the ostwald process. *Physical Review X* **8**, 031080 (2018).
20. Wittmann, R., Smallenburg, F. & Brader, J. M. Pressure, surface tension, and curvature in active systems: A touch of equilibrium. *The Journal of chemical physics* **150** (2019).
21. Omar, A. K., Wang, Z.-G. & Brady, J. F. Microscopic origins of the swim pressure and the anomalous surface tension of active matter. *Phys. Rev. E* **101**, 012604 (2020). URL <https://link.aps.org/doi/10.1103/PhysRevE.101.012604>.
22. Wysocki, A. & Rieger, H. Capillary action in scalar active matter. *Phys. Rev. Lett.* **124**, 048001 (2020). URL <https://link.aps.org/doi/10.1103/PhysRevLett.124.048001>.

23. Fausti, G., Tjhung, E., Cates, M. E. & Nardini, C. Capillary interfacial tension in active phase separation. *Phys. Rev. Lett.* **127**, 068001 (2021). URL <https://link.aps.org/doi/10.1103/PhysRevLett.127.068001>.
24. Turci, F. & Wilding, N. B. Wetting transition of active brownian particles on a thin membrane. *Phys. Rev. Lett.* **127**, 238002 (2021). URL <https://link.aps.org/doi/10.1103/PhysRevLett.127.238002>.
25. Neta, P. D., Tasinkevych, M., Telo da Gama, M. M. & Dias, C. S. Wetting of a solid surface by active matter. *Soft Matter* **17**, 2468–2478 (2021). URL <http://dx.doi.org/10.1039/D0SM02008G>.
26. Adkins, R. *et al.* Dynamics of active liquid interfaces. *Science* **377**, 768–772 (2022).
27. Caballero, F. & Marchetti, M. C. Activity-suppressed phase separation. *Physical Review Letters* **129**, 268002 (2022).
28. Tayar, A. M. *et al.* Controlling liquid–liquid phase behaviour with an active fluid. *Nature Materials* **22**, 1401–1408 (2023).
29. Rojas-Vega, M., de Castro, P. & Soto, R. Wetting dynamics by mixtures of fast and slow self-propelled particles. *Phys. Rev. E* **107**, 014608 (2023). URL <https://link.aps.org/doi/10.1103/PhysRevE.107.014608>.
30. Li, L., Sun, Z. & Yang, M. Surface tension between coexisting phases of active brownian particles. *arXiv preprint arXiv:2308.04917* (2023).

31. Mangeat, M., Chakraborty, S., Wysocki, A. & Rieger, H. Stationary particle currents in sedimenting active matter wetting a wall. *Phys. Rev. E* **109**, 014616 (2024). URL <https://link.aps.org/doi/10.1103/PhysRevE.109.014616>.
32. Solon, A. P. *et al.* Pressure is not a state function for generic active fluids. *Nature physics* **11**, 673–678 (2015).
33. Zakine, R. *et al.* Surface tensions between active fluids and solid interfaces: Bare vs dressed. *Phys. Rev. Lett.* **124**, 248003 (2020). URL <https://link.aps.org/doi/10.1103/PhysRevLett.124.248003>.
34. Hermann, S., de las Heras, D. & Schmidt, M. Non-negative interfacial tension in phase-separated active brownian particles. *Phys. Rev. Lett.* **123**, 268002 (2019). URL <https://link.aps.org/doi/10.1103/PhysRevLett.123.268002>.
35. Lauersdorf, N., Kolb, T., Moradi, M., Nazockdast, E. & Klotsa, D. Phase behavior and surface tension of soft active brownian particles. *Soft Matter* **17**, 6337–6351 (2021).
36. Fily, Y. & Marchetti, M. C. Athermal phase separation of self-propelled particles with no alignment. *Physical review letters* **108**, 235702 (2012).
37. Redner, G. S., Hagan, M. F. & Baskaran, A. Structure and dynamics of a phase-separating active colloidal fluid. *Biophysical Journal* **104**, 640a (2013).
38. Cates, M. E. & Tailleur, J. Motility-induced phase separation. *Annu. Rev. Condens. Matter Phys.* **6**, 219–244 (2015).

39. Kirkwood, J. G. & Buff, F. P. The statistical mechanical theory of surface tension. *The Journal of Chemical Physics* **17**, 338–343 (1949).
40. Navascués, G. & Berry, M. The statistical mechanics of wetting. *Molecular Physics* **34**, 649–664 (1977).
41. Solon, A. P., Stenhammar, J., Cates, M. E., Kafri, Y. & Tailleur, J. Generalized thermodynamics of motility-induced phase separation: phase equilibria, laplace pressure, and change of ensembles. *New Journal of Physics* **20**, 075001 (2018).
42. Fily, Y., Kafri, Y., Solon, A. P., Tailleur, J. & Turner, A. Mechanical pressure and momentum conservation in dry active matter. *Journal of Physics A: Mathematical and Theoretical* **51**, 044003 (2017).
43. Schnitzer, M. J. Theory of continuum random walks and application to chemotaxis. *Physical Review E* **48**, 2553 (1993).
44. Szamel, G. Self-propelled particle in an external potential: Existence of an effective temperature. *Physical Review E* **90**, 012111 (2014).
45. Solon, A. P. *et al.* Pressure and phase equilibria in interacting active brownian spheres. *Physical review letters* **114**, 198301 (2015).
46. Yang, X., Manning, M. L. & Marchetti, M. C. Aggregation and segregation of confined active particles. *Soft matter* **10**, 6477–6484 (2014).

47. Takatori, S. C., Yan, W. & Brady, J. F. Swim pressure: stress generation in active matter. *Physical review letters* **113**, 028103 (2014).
48. Solon, A. P., Stenhammar, J., Cates, M. E., Kafri, Y. & Tailleur, J. Generalized thermodynamics of motility-induced phase separation: phase equilibria, Laplace pressure, and change of ensembles. *New Journal of Physics* **20**, 075001 (2018).
49. Das, S., Gompper, G. & Winkler, R. G. Local stress and pressure in an inhomogeneous system of spherical active brownian particles. *Scientific reports* **9**, 6608 (2019).
50. Speck, T. Coexistence of active brownian disks: Van der waals theory and analytical results. *Physical Review E* **103**, 012607 (2021).
51. Omar, A. K., Row, H., Mallory, S. A. & Brady, J. F. Mechanical theory of nonequilibrium coexistence and motility-induced phase separation. *Proceedings of the National Academy of Sciences* **120**, e2219900120 (2023). URL <https://www.pnas.org/doi/abs/10.1073/pnas.2219900120>. <https://www.pnas.org/doi/pdf/10.1073/pnas.2219900120>.
52. Speck, T. Collective forces in scalar active matter. *Soft Matter* **16**, 2652–2663 (2020).
53. Langford, L. & Omar, A. K. Theory of capillary tension and interfacial dynamics of motility-induced phases. *arXiv preprint arXiv:2308.08531* (2023).
54. Wilhelmy, L. Ueber die abhängigkeit der capillaritäts-constanten des alkohols von substanz und gestalt des benetzten festen körpers. *Annalen der Physik* **195**, 177–217 (1863).

55. Pockels, A. Relations between the surface-tension and relative contamination of water surfaces. *Nature* **48**, 152–154 (1893).
56. Du Noüy, P. L. A new apparatus for measuring surface tension. *The Journal of general physiology* **1**, 521 (1919).
57. Volpe, C. D. & Siboni, S. The wilhelmy method: a critical and practical review. *Surface Innovations* **6**, 120–132 (2018).
58. Angelani, L., Maggi, C., Bernardini, M., Rizzo, A. & Di Leonardo, R. Effective interactions between colloidal particles suspended in a bath of swimming cells. *Physical review letters* **107**, 138302 (2011).
59. Ray, D., Reichhardt, C. & Reichhardt, C. O. Casimir effect in active matter systems. *Physical Review E* **90**, 013019 (2014).
60. Rohwer, C. M., Kardar, M. & Krüger, M. Transient casimir forces from quenches in thermal and active matter. *Physical review letters* **118**, 015702 (2017).
61. Baek, Y., Solon, A. P., Xu, X., Nikola, N. & Kafri, Y. Generic long-range interactions between passive bodies in an active fluid. *Phys. Rev. Lett.* **120**, 058002 (2018). URL <https://link.aps.org/doi/10.1103/PhysRevLett.120.058002>.
62. Granek, O., Baek, Y., Kafri, Y. & Solon, A. P. Bodies in an interacting active fluid: Far-field influence of a single body and interaction between two bodies. *arXiv preprint arXiv:1912.07623* (2019).

63. Kjeldbjerg, C. M. & Brady, J. F. Theory for the casimir effect and the partitioning of active matter. *Soft Matter* **17**, 523–530 (2021).
64. Granek, O. *et al.* Inclusions, boundaries and disorder in scalar active matter. *In Press at Rev. Mod. Phys.*, *arXiv preprint arXiv:2310.00079* (2024).
65. Speck, T. & Jack, R. L. Ideal bulk pressure of active brownian particles. *Physical Review E* **93**, 062605 (2016).
66. Fins Carreira, A. *et al.* How to steer active colloids up a vertical wall. *Nature Communications* **15**, 1710 (2024).
67. Douezan, S. *et al.* Spreading dynamics and wetting transition of cellular aggregates. *Proceedings of the National Academy of Sciences* **108**, 7315–7320 (2011).
68. Joanny, J. F., Kruse, K., Prost, J. & Ramaswamy, S. The actin cortex as an active wetting layer. *The European Physical Journal E* **36**, 1–6 (2013).
69. Pérez-González, C. *et al.* Active wetting of epithelial tissues. *Nature physics* **15**, 79–88 (2019).
70. Agudo-Canalejo, J. *et al.* Wetting regulates autophagy of phase-separated compartments and the cytosol. *Nature* **591**, 142–146 (2021).
71. Mangiarotti, A., Chen, N., Zhao, Z., Lipowsky, R. & Dimova, R. Wetting and complex remodeling of membranes by biomolecular condensates. *Nature Communications* **14**, 2809 (2023).

72. Junot, G., Briand, G., Ledesma-Alonso, R. & Dauchot, O. Active versus passive hard disks against a membrane: mechanical pressure and instability. *Physical review letters* **119**, 028002 (2017).